Particle Transport in Vanishing Turbulence Conditions in the Tore Supra Plasma Core

R. Guirlet, A. Sirinelli[1], T. Parisot[2], R. Sabot, X. Garbet, J.F. Artaud, C. Bourdelle, P. Hennequin*, G.T. Hoang, F. Imbeaux, J.L. Ségui, D. Villegas

CEA, IRFM, F-13108 Saint-Paul-Lez-Durance, France
*Laboratoire de Physique des Plasmas, CNRS-Ecole Polytechnique,91128 Palaiseau Cedex, France

E-mail contact of main author: remy.guirlet@cea.fr

Abstract: Electron and impurity transport has been studied in sawtoothing plasmas in the Tore Supra tokamak. High time and space resolution measurements of the electron density reveal the existence of a flat profile region encompassing the q = 1 surface, on which is superimposed a density peak building up between sawtooth relaxations. Transport of both nickel and electrons has been determine independently of the effect of sawteeth in the central part of the plasma. In the core, electron transport exceeds the neoclassical values as calculated with the NCLASS code, although the turbulence level is very low. In contrast, nickel transport is in good agreement with the neoclassical calculations in the whole central region. The neoclassical effect on trapped particles of a persisting mode due to incomplete reconnection of the magnetic surfaces is consistent with these observations.

1. Introduction

The observed transport of charged particles in tokamaks is usually attributed to the effect of collisions [1, 2] and turbulence ([3] and references therein) on trapped or passing particles. Although the effect of a non-axisymmetric field has been investigated in momentum transport studies [4, 5], the collisional transport predictions for particles generally assume an axisymmetric magnetic field. We report here a series of observations of electron and impurity transport, the former exceeding and the latter matching the axisymmetric neoclassical expectations in ohmic, sawtoothing plasmas [6]. The relationship between these experimental results and the electron density fluctuations measurements is discussed. The possible role of the magnetic perturbation associated with the sawtooth activity is discussed.

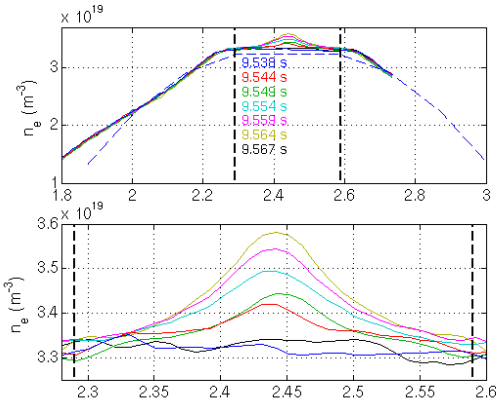

Figure 1: Sample of density profiles as measured by the reflectometer over a sawtooth period. (top) Full radial profile, (bottom) close-up on the central part of the profile. Dashed line: interferometer measurement in the same time interval (discharge TS#35035). Vertical dashed lines: q = 1 surface.

2. Electron transport

2.1. Observations

Measurements evidencing a narrow central density peak are common in ohmic Tore-Supra discharges [7]. In order to follow the temporal evolution of the plasma core during the build-up phase of a

[1] Present address: EURATOM/CCFE Fusion Association, Culham Science Centre, Abingdon, Oxon OX14 3DB, United Kingdom
[2] Present address: Laboratoire Arc Electrique et Plasmas Thermiques, Université Blaise Pascal, Clermont-Ferrand, France

sawtooth, we measure a few hundreds profiles with the D-band reflectometer [8, 9] at a high repetition rate of 13 to 25 kHz. Figure 1 shows a sample of the profiles measured in an ohmic discharge at I_P = 1 MA during a 30 ms sequence (approximately a sawtooth period). The good space and time resolutions of the reflectometer reveals that the density peaking consists of a very local steepening of the profile close to the magnetic axis on top of a central plateau region. The central peak in the core region grows almost linearly during the sawtooth while the density of the plateau and that in the gradient area do not evolve. The growth of the central peak is stopped by the sawtooth crash (Fig. 2), which leads back to a flat core.

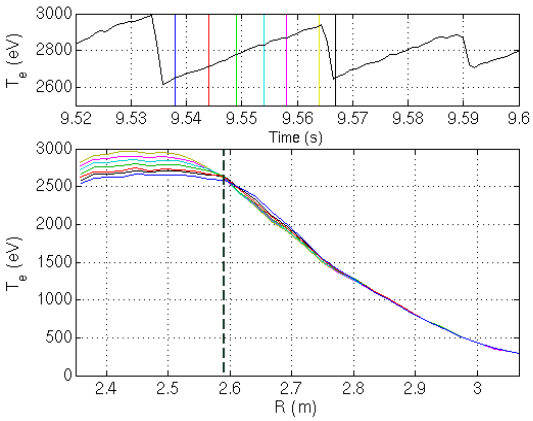

Figure 2: (Top) time evolution of the measured central temperature. Vertical lines indicate times of the profiles shown below and in figure 1. (Bottom) electron temperature profile evolution. Dashed black line: sawtooth inversion radius deduced from ECE.

The density at the peak can represent up to 10% of the plateau density and it has a typical width of 15 cm ($\Delta r/a \sim 0.2$). As can be seen in Fig. 2 (bottom) no such peaking is observed for the temperature This density peak cannot be caused by particle source since there is no plasma fuelling in the plasma core (see [10] and next section).

Plasma current (I_P) scan experiments have been performed to explore the link between the plateau and peak structure and the radius of the q = 1 surface. The latter is determined in the following way. The current diffusion equation is solved in CRONOS using the neoclassical resistivity, *(i)* from the T_e profiles fitted from both ECE and Thomson scattering measurements, *(ii)* assuming a flat Z_{eff} profile. This technique allows an accurate reconstruction of the current profile in these ohmic discharges.

For each I_P step, density and temperature profiles have been analysed. The measured widths of the density peak and of the density plateau are shown in Figure 3 as a function of the q = 1 surface radius and of the plasma current. Above I_P = 0.8 MA, the width of the density peak saturates with increasing current. At I_P = 500 kA, the central density peaking is not observed. It may be explained by the fact that the q = 1 surface radius is then smaller than the usual peak width. There is a clear correlation between the width of the plateau and the plasma current. The density plateau width increases with increasing I_P and always extends beyond the q = 1 surface. Such a density flattening could be due to an increased particle diffusion coefficient or to an outward turbulent convective flux. However, this plateau is not observed on the temperature profile, as can be seen on the radial temperature profiles measured by the ECE radiometer (Figure 2) and the turbulence level measured by reflectometry remains low in this region (Figure 4). An alternative explanation could be the presence of convective cells

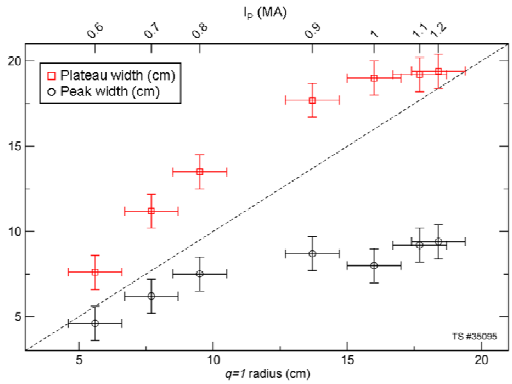

Figure 3: Central plateau width (defined as shown in figure 1) and density peak FWHM as a function of the q = 1 surface radius during an I_p scan.

around the $q = 1$ surface, due to low magnetic shear, as suggested by [11]. At this stage, no firm conclusion can be drawn.

2.2. Radial electron transport analysis

The density profile evolves spontaneously between sawtooth crashes. This feature, together with the time resolution of the density measurements by reflectometry, which is much better than the typical time scale of a sawtooth, made possible the determination of the experimental electron transport coefficients in the core of an ohmic, sawtoothing plasma without any external perturbation of the plasma. No transport code is used and the only hypothesis is that the transport coefficients are independent of time between sawtooth crashes.

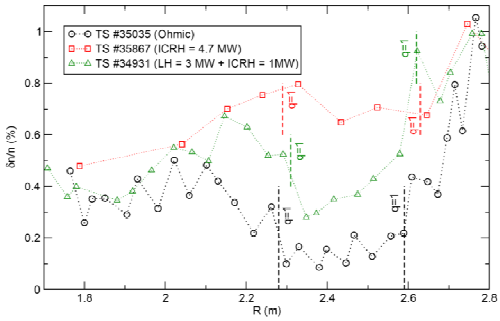

Figure 4: Density fluctuations measured by reflectometry in an ohmic discharge, compared with ICRH and LHCD heated discharges. Dashed lines: q = 1 surface location.

Let us make the usual assumption that the electron flux is the sum of a diffusive term and a convective term. This assumption implies that Γ_e/n_e is linear in $\nabla n_e/n_e$:

$$\Gamma_e / n_e = -D_e \nabla n_e / n_e + V_e$$

where D_e and V_e are the electron diffusion coefficient and convection velocity respectively. If the electron transport coefficients are constant in time, the evaluation of Γ_e/n_e as a function of $\nabla n_e/n_e$ at a given radius allows us to obtain the transport coefficients D_e and V_e, from the slope and intercept of the curve $\Gamma_e/n_e = f(-\nabla n_e/n_e)$ respectively.

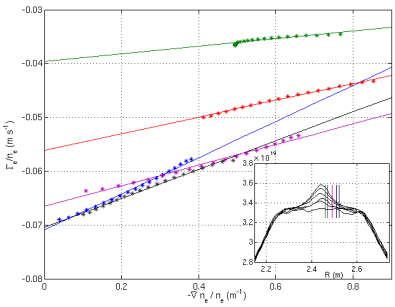

***Figure 5**: Γ_e/n_e as a function of $\nabla n_e/n_e$ at five radii among the 20 used in the analysis. The transport coefficients D and V are the slope and the intercept of the linear fits of the experimental points. Symbols: averages of the measured profile over 1 ms (see section 2.4). Inset shows radii displayed on the main figure.*

The electron flux can be obtained through the continuity equation :

$$\partial_t n_e + \vec{\nabla}.\vec{\Gamma}_e = S_e$$

where S_e is the external electron source. As S_e cannot be measured, we have calculated it with the one-dimensional code METIS [12] which assumes a diffusion coefficient constructed from the neutral velocity and mean free path and takes into account electron impact ionisation of neutrals and charge exchange processes of neutrals with plasma ions. In the region we analyse here ($r/a \leq 0.15$), the calculated source is lower by at least four orders of magnitude than what would be required to sustain the measured central density (a more refined source calculation with the 3-dimension code Eirene [13] in a plasma at a slightly lower density led to the same conclusion [10]). In other words, the evolution of the central density profile can be considered to be entirely governed by transport. We can thus neglect the source term in the continuity equation :

$$\partial_t n_e + \vec{\nabla}.\vec{\Gamma}_e = 0$$

and obtain the electron flux by integrating it over radius in cylindrical geometry :

$$\Gamma_e(r) = -\frac{1}{r}\int_0^r r' \partial_t n_e dr'.$$

The density gradient is determined directly from the density profiles measured by reflectometry after removal of the effect of a rotating mode (the uncertainty associated with this procedure is evaluated in Section 2.3).
During a sawtooth period, $\Gamma_e(r,t)/n_e$ and $\nabla n_e/n_e$ are determined at about 20 radial points, half of which on the high field side and the other half on the low field side. In Figure 5, $\Gamma_e/n_e = -D_e \nabla n_e/n_e + V_e$ is represented as a function of $-\nabla n_e/n_e$ for the particular sawtooth analysed here (only five radii are shown for clarity). At all radii the points deduced from the measurements are well aligned on a straight line, which justifies *a posteriori* the hypothesis of constant transport coefficients. The electron transport coefficients D_e and V_e are respectively the slope and the intercept of the line fitted to the experimental points at each radius. The good time resolution compared to the time window width allows very small uncertainties (less than 10^{-4} m^2/s and 10^{-4} m/s resp.) compared with the other sources of error listed in the next section.

Figure 6 shows the D_e and V_e profiles obtained with this method. The radial interval displayed on the figure is intentionally limited to about 10 cm ($r/a \sim 0.15$) on both the high and low field sides. Further from the magnetic axis the density profile is almost flat and constant in time. The flatness of the profile makes the normalised density gradient difficult to evaluate and the fact that it is constant produces large uncertainties in the particle flux.

Close to the magnetic axis, the values of both the normalised gradient and the electron flux tend to 0. They are thus affected by large uncertainties which, in the present case, result in erroneous negative values of the diffusion coefficient. In the gradient region, the method gives larger values of D_e (up to 0.2 to 0.4 m^2/s around $r/a = 0.5$) and V_e (around 0.2 m/s) but with spurious spikes probably due to the fact that the method has not been optimised for this plasma region. Nevertheless, the global picture is that of reduced electron transport in the plasma centre compared with the gradient region. These results are compared with theoretical transport predictions in Section 4.

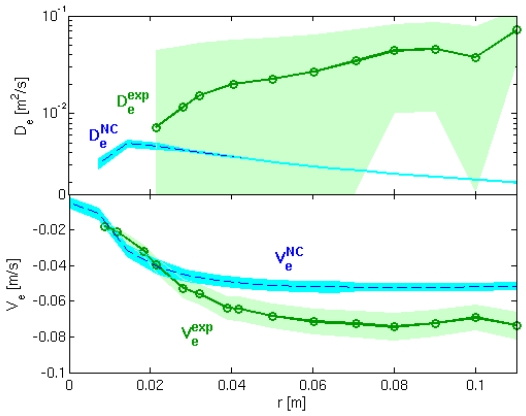

Figure 6: *Diffusion coefficient De (top) and convection velocity Ve (bottom). Solid line: experimental coefficients deduced from the preceding figure, dashed line: corresponding neoclassical coefficients calculated by the NCLASS code [20] included in the CRONOS package [23]. The shaded areas represent the error bars as evaluated in section 2.3.*

2.3. Uncertainties

Various error sources have been investigated. The corresponding uncertainties are summarised in the table below. First, in the scenario of the present experiment, the density measurements as a function of the major radius (*i.e.* the distance from the measurement point to the symmetry axis of the machine) commonly reveal a fluctuation of the maximum density position with an amplitude of about 4-5 cm. It is attributed to a rotating mode of odd parity, most probably a ($m = 1$, $n = 1$) mode. Another source of error is the small asymmetry of the experimental values of D and V on either side of the magnetic axis. The most likely explanation is the uncertainty in the magnetic equilibrium reconstruction together with the sensitivity of the flux-gradient method. The boundaries of the time window over which the analysis is performed also has an influence on the results, maybe due to residual MHD modes after the sawtooth relaxations.

Error source	δD_e (m^2/s)	δV_e(m/s)
Rotating mode (evaluated at r/a ~ 0.08)	0.02	5×10^{-3}
HFS/LFS asymmetry	7×10^{-3}	2.5×10^{-3}
Time window boundaries	-0.02, +0.03	-0.015, +0.007
Sawtooth variability	0.01	5×10^{-3}
Error on minor radius of measurement points	negligible	

The various error sources can roughly be considered as independent from each other. The total uncertainties on the diffusion coefficient and the convection velocity can thus be calculated as follows :

$$\delta D_{tot} = \sqrt{(\delta D_{rot})^2 + (\delta D_{FS})^2 + (\delta D_{TW})^2 + (\delta D_{stat})^2},$$

$$\delta V_{tot} = \sqrt{(\delta V_{rot})^2 + (\delta V_{FS})^2 + (\delta V_{TW})^2 + (\delta V_{stat})^2}.$$

They have been calculated at each radial point taking into account the radial dependence of the various error sources. They are of the order of 3×10^{-2} m^2/s and 1.2×10^{-2} m/s.

Transport coefficient profiles have been generated within these uncertainties to reconstruct the density profile evolution. The comparison with the measured profiles shows that the error bar on D_e represents fairly well the domain compatible with the measurements while that on V_e is slightly overestimated. A value of $\delta V_e / V_e \sim 10\%$ is more consistent with the measurements.

2.4. Theoretical transport calculations

Neoclassical and turbulent transport calculations have been performed by running NCLASS [14] and the quasilinear gyrokinetic model QuaLiKiz [15, 16] respectively, with an integrated modelling of the plasma by CRONOS [17]. The neoclassical transport coefficients are shown in Fig. 6 with error bars calculated by varying the electron density and temperature by the measurement uncertainty (5%) around their measured values. According to QuaLiKiz, turbulent micro-instabilities are expected to develop outside a central region defined approximately by the $q = 1$ surface but not inside this region, because the gradients are below the calculated thresholds. This prediction is in agreement with the measured density fluctuation level (shown in Fig. 4) which is very low (about 0.2%) within the $q = 1$ surface, with a sharp transition to substantially higher values outside this surface. The calculated transport coefficients are thus in contrast with the experimental electron diffusion coefficient (and, to a lesser extent, the convection velocity), which is unambiguously higher than predicted by NCLASS in most of the central region. Only very close to the magnetic axis do the experimental results meet the NCLASS calculations (within a rather large error bar for diffusion). This is further discussed in Section 4.

3. Impurity transport

3.1. Experiment and radial impurity transport analysis

The scenario chosen to study impurity transport in the presence of sawteeth is similar to that used in [18], the novelty being in the way sawteeth are taken into account in the analysis, as explained below (and originally in [19]). Traces of Nickel were injected by laser blow-off. Contrary to the electron transport analysis presented in Section 2, which could not be performed on a time scale larger than the sawtooth period, the impurity analysis can be and is always performed on a time interval of a few particle confinement times in order to minimise the error bars. In order to distinguish the redistributing effects of the sawtooth

relaxations, which are not the object of this work, from the 'pure transport' effects, it is necessary to process in two steps.

First, the background plasma soft-X ray emission is subtracted from the measurements using its strong relationship with the plasma temperature. The remaining signal represents the emission of the injected species only. It is also affected by sawteeth and is thus processed using the model of [20]. The relaxations are assumed to flatten the impurity density profile instantaneously inside the $q = 1$ surface radius $r_{q=1}$. Outside a minor radius r_{mix} slightly larger than $r_{q=1}$, sawteeth are assumed to be ineffective. The number of particles being invariant, the only parameter of this model is the mixing radius r_{mix}. Its value is of the order of $1.2 \times r_{q=1}$.

Between the sawtooth relaxations, the standard iterative procedure based on the continuity equation resolution [21] was applied. This first step revealed a strong contrast between a weak transport region around the magnetic axis and the outer plasma characterised by strong transport diffusion. Instead of the automatic optimisation algorithm [22], the step-by-step optimisation algorithm [23] designed for impurity transport determination has been used in the present case, since we wanted to control every step of the process. The drawback of this method is that it was not possible to determine the uncertainties on the experimental transport coefficients.

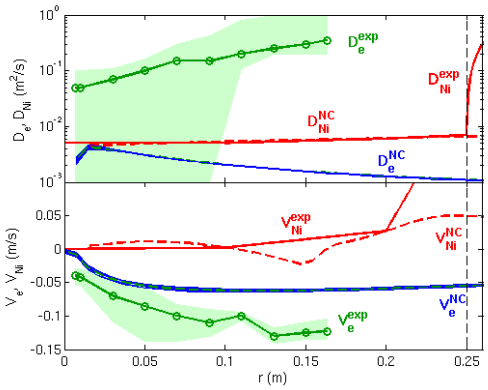

Figure 7. *Experimental and neoclassical (NCLASS) diffusion coefficient (top) and convection velocity (bottom) for the discharge with a Ni injection (TS#36782). Solid lines: experimental results, dashed line: neoclassical calculations of NCLASS. Coloured bands: uncertainties on the experimental electron coefficients due to the sawtooth variability. Vertical dashed line: sawtooth inversion radius.*

The transport coefficient profiles can be seen in Fig. 7. The analysed region extends further than for electrons but with a poorer radial resolution, because of the relative lack of localised measurements but also of the analysis method. The profiles show a very sharp transition at $r \sim 0.25$ m, which coincides with the sawtooth inversion radius observed on the ECE measurements. Further outside, the diffusion coefficient is more than two orders of magnitude higher than the NCLASS prediction, with a substantial inward convective flux. The contrast with the results of Section 2.2 concerning electron transport makes a detailed comparison necessary.

3.3. Comparison with electron transport

As the reader may have noticed, the scenario used for the impurity study is at higher density than that for electrons. We have thus performed again the electron transport analysis on the impurity-seeded discharge. We have used the method described in Section 2.2, the poorer reflectometry time sampling (4 ms instead of 75 µs in Section 2) being partly compensated by the possibility of analysing five sawteeth (thanks to the longer acquisition time interval) instead of only one as in Section 2.2.

The resulting D_e and V_e profiles are shown in Fig. 7. The coloured band indicates the error bars defined by the extreme values of the coefficients found at each radius. The D_e and V_e profiles have a shape very similar to those obtained with the detailed analysis in Section 2.2 but with somewhat higher values. Note that here the experimental values are above the

NCLASS predictions, even close to the magnetic axis. Note also that, despite the rather large error bars, we observe $D_e > D_{Ni}$ inside the $q = 1$ surface.

4. Interpretation

In order to recover consistency between the theoretical models and the experimental results, we suggest two processes which could complete the axisymmetric neoclassical and turbulent transport models. Both processes are based on the effect of the magnetic perturbation of the rotating mode (see description in Section 2.3) on trapped particles and can be deduced from the calculations in [24] and references therein. The radial displacement ξ of the magnetic surfaces is related to the parallel component of the magnetic field perturbation (the only component relevant for transport) in the following way:

$$\delta \approx \beta \frac{\xi}{L_p},$$

where $\delta = \delta B_{//}/B$, L_p is the pressure gradient length and β is the kinetic pressure to magnetic pressure ratio. With common values of β and L_p, we obtain approximately $2\times10^{-3} \le \delta \le 10^{-2}$.

The first possible effect which we have calculated is that of particles trapped in the magnetic perturbation. The relevant collisionality parameter $\nu_{ripple,s}^* = \delta^{3/2}\nu_s / \omega_{T,s}$ (where ν_s is the collision frequency and $\omega_{T,s} = (1-1/q)v_{T,s}/R$ the trapped particle transit frequency for a species s) is larger than one for electrons, which means that they are in the plateau regime. The diffusion coefficient associated with these helically trapped particles is of the form :

$$D_{HP,s} = \left(\frac{\delta}{\varepsilon}\right)^2 \frac{qR}{1-q}\frac{v_{D,s}^2}{v_{T,s}}$$

where $\varepsilon = r/R$ is the inverse aspect ratio and $v_{D,s}$ the particle vertical drift velocity. With central values of $n_e \sim 3.5\times10^{19}$ m^{-3} and $T_e \sim 2.5$ keV, we obtain $D_{HP,e} \sim (10\text{-}50)\times\delta^2$ m^2/s, *i.e.* between 10^{-4} and 5×10^{-3} m^2/s. These values are of the order of (or slightly smaller than) the NCLASS diffusion coefficient of electrons (a few 10^{-3} m^2/s, as can be seen in Fig 6). This effect can thus contribute substantially the observed diffusion coefficient.

Assuming a charge of 26 for nickel around the magnetic axis, the same effect for the nickel ions has been evaluated. Nickel is also in the plateau regime and using the same formula as for electrons, we find $D_{HP,Ni} \sim 0.2\times D_{HP,e} < 10^{-3}$ m^2/s, which is small compared to the NCLASS prediction and the observed value (see Fig. 7).

The second effect comes from the contribution of the curvature drift due to the magnetic perturbation on the particles trapped in the main magnetic field. The relevant electron collisionality parameter, ν_e/ε, indicates that our situation corresponds to the so-called banana-drift regime, for which the diffusion coefficient is given by :

$$D_{BD,e} \approx \frac{\delta^2}{\sqrt{\varepsilon}}\frac{v_{D,e}^2}{\nu_e}.$$

In the present case, we have $D_{BD,e} \sim 30\times\delta^2$ m^2/s. It is of the same order of magnitude as $D_{HP,e}$ and thus can also contribute substantially the observed value.

The same effect calculated for the nickel ions shows that Nickel is in the so-called 'ripple-plateau' regime, for which the diffusion coefficient is :

$$D_{RP,Z} \approx \left(\frac{q\delta}{\varepsilon}\right)^2 \frac{qR}{1-q}\times\frac{v_{D,Z}^2}{v_{T,Z}} \approx q^2 D_{HP,Z}.$$

In the central part of the plasma, where q is close to 1, it is thus close to $D_{HP,Z}$ and significantly smaller than the NCLASS prediction and the observed value.

In summary, the non-axisymmetrical neoclassical effect of the magnetic perturbation associated with the rotating mode is a good candidate to explain the experimental observations. It has a substantial effect on electron transport which indeed is observed to be stronger than predicted by NCLASS, whereas it has a small effect on Nickel transport which is ibserved to be in good agreement with the NCLASS predictions.

5. Conclusion

Investigation of electron and Nickel transport was performed in plasmas affected by sawteeth. For the first time in this regime, the underlying transport of electrons and impurities was determined independently of the effect of sawtooth relaxations. Thanks to the existence of a central density peak evolving between the sawtooth relaxations, electron transport could be deduced in the central plasma region ($r/a \leq 0.2$) from the linear relationship between the electron flux normalised to density and the inverse electron density gradient length, without the help of a modelling code. Nickel transport has been determined by solving the system of coupled continuity equations of all the nickel ionisation stages, with a heuristic model of particle redistribution due to the sawtooth crashes.

The radial transport analysis performed on the core density profiles between sawtooth crashes shows that the electron diffusion coefficient and convection velocity within the $q = 1$ surface are larger than the NCLASS predictions. This is in contrast both with the very low measured fluctuation level in the same region and with the gyrokinetic linear stability analysis indicating that the core plasma gradients are below the thresholds. In contrast, nickel transport is in very good agreement with the NCLASS predictions in this volume.

The non-axisymmetric, neoclassical effect of an odd parity, probably ($m = 1$, $n = 1$), rotating mode between the sawtooth relaxations is a good candidate to explain these observations. It is shown to be significant and consistent with the observations for electrons while it is estimated to have little effect on nickel.

This work, supported by the European Communities under the contract of Association between EURATOM and CEA, was carried out within the framework of the European Fusion Development Agreement. The views and opinions expressed herein do not necessarily reflect those of the European Commission.

[1] Hinton F.L. and Hazeltine R.D., Rev. Mod. Phys. **48**, 239 (1976).
[2] Hirshman S.P. and Sigmar D.J., Nucl. Fusion **21**, 1079 (1981).
[3] Garbet X. et al., Nucl. Fusion **50**, 043002 (2010).
[4] LaBombard B. *et al.*, Nucl. Fusion **44**, 1047 (2004).
[5] Garofalo A.M. *et al.*, Phys. Rev. Lett. **101**, 195005 (2008).
[6] Guirlet R. et al., Nucl. Fusion 50, 095009 (2010).
[7] Sabot S. *et al.*, Plasma Phys. Control. Fusion, **48** B421 (2006).
[8] Clairet F. *et al.*, Plasma Phys. Control. Fusion, **43** 429 (2001).
[9] Sabot S. *et al.*, Nucl. Fusion, **46**, S685 (2006).
[10] Hoang G.T. *et al.*, Phys. Rev. Lett. **90**, 155002 (2003).
[11] De Blank H.J. and Schep T.J., Phys. Fluids B **3**, 1136 (1991).
[12] Laporte P., PhD Thesis, Université de Provence, France (1996).
[13] Reiter D. *et al.*, Fusion Sci. Technol. **47**, 172 (2005).
[14] Houlberg W.A. *et al.*, Phys. Plasmas **4**, 3230 (1997).
[15] Bourdelle C. *et al.*, Phys. Plasmas **14**, 112501 (2007).
[15] Casati A. *et al.*, Nucl. Fusion **49**, 085012 (2009).
[17] Artaud J.F. *et al.*, Nucl. Fusion **50**, 043001 (2010).
[18] Mattioli M. *et al.*, Nucl. Fusion **38**, 1629 (1998).
[19] Parisot T., PhD Thesis, Université de Provence, France (2007).
[20] Ida K. *et al.*, Phys. Rev. Lett. **58**, 116 (1987).
[21] Guirlet R. *et al.*, Nucl. Fusion **49**, 055007 (2009).
[22] Villegas D. *et al.*, P4.209, 36th EPS Conference on Plasma Phys. Control. Fusion, Sofia (2009).
[23] Parisot Th. *et al.*, Plasma Phys. Control. Fusion **50**, 055010 (2008).
[24] Garbet X. *et al.*, Phys. Plasmas 17, 072505 (2010).